Rev. Adv. Mater. Sci. 52 (2017) 5-13

EFFECT OF COOPERATIVE GRAIN BOUNDARY SLIDING AND MIGRATION ON FRACTURE TOUGHNESS OF NANOSTRUCTURED SOLIDS WITH INCLUSIONS

S.V. Bobylev[1,2,3], A.S. Kochnev[2] and N.V. Skiba[1,2,3]

[1]Peter the Great St. Petersburg Polytechnic University, St. Petersburg 195251, Russia
[2]St. Petersburg State University, St. Petersburg 199034, Russia
[3]Institute of Problems of Mechanical Engineering, Russian Academy of Sciences, St. Petersburg, 199178, Russia

Received: September 12, 2017

Abstract. A new mechanism of fracture toughness enhancement in nanostructured materials containing inclusions of the second phase is suggested. The mechanism represents the cooperative grain boundary (GB) sliding and stress-driven GB migration process near the tips of growing cracks. It is shown that this mechanism can increase the critical stress intensity factor for crack growth in nanostructured materials with inclusions by a factor of two or more and thus considerably enhances the fracture toughness of such materials.

1. INTRODUCTION

Nanostructured materials exhibit outstanding mechanical properties (first of all, superior strength), which are highly important for a range of structural and functional applications; see, e.g., [1-10]. These properties are crucially influenced by plastic deformation mechanisms/modes operating in such materials and having specific features due to large amounts of grain boundaries in such materials. In particular, stress-driven migration of grain boundaries (GBs) represents one of grain boundary deformation modes effectively operating in nanostructured materials [11-35].

Up to now, some rather impressive progress has been achieved in experimental identification, computer simulations and theoretical description of deformation processes occurring through the stress-driven migration of grain boundaries nanocrystalline materials with a homogeneous chemical structure. At the same time, research of the stress-driven migration of grain boundaries in such chemically inhomogeneous materials as nanostructured metals containing inclusions of the second phase is limited. Recently, we proposed several theoretical models [13,14,18,28,29] describing stress-driven migration in metal-based composites (specifically metal-graphene composites). In fact the same models is applicable not only to metal-graphene composites, but also to any metals containing inclusions of the second phase. For example, Al-matrix and Al-alloy-matrix nanocomposites with ceramic Al_2O_3 inclusions [36,37], or metallic alloys with metallic nanoinclusions [38-41] like Al-3Mg-0.2Sc alloy, containing Al_3Sc precipitates used as model system in the theoretical model [28].

In the above mentioned theoretical models [13,14,18,28,29] we considered exclusively stress-driven GB migration. But it is known from earlier works [11,12,30], that GB migration is often accompanied by GB sliding and both mechanisms can effectively accommodate each other effectively en-

Corresponding author: Sergey V. Bobylev, e-mail: bobylev.s@gmail.com

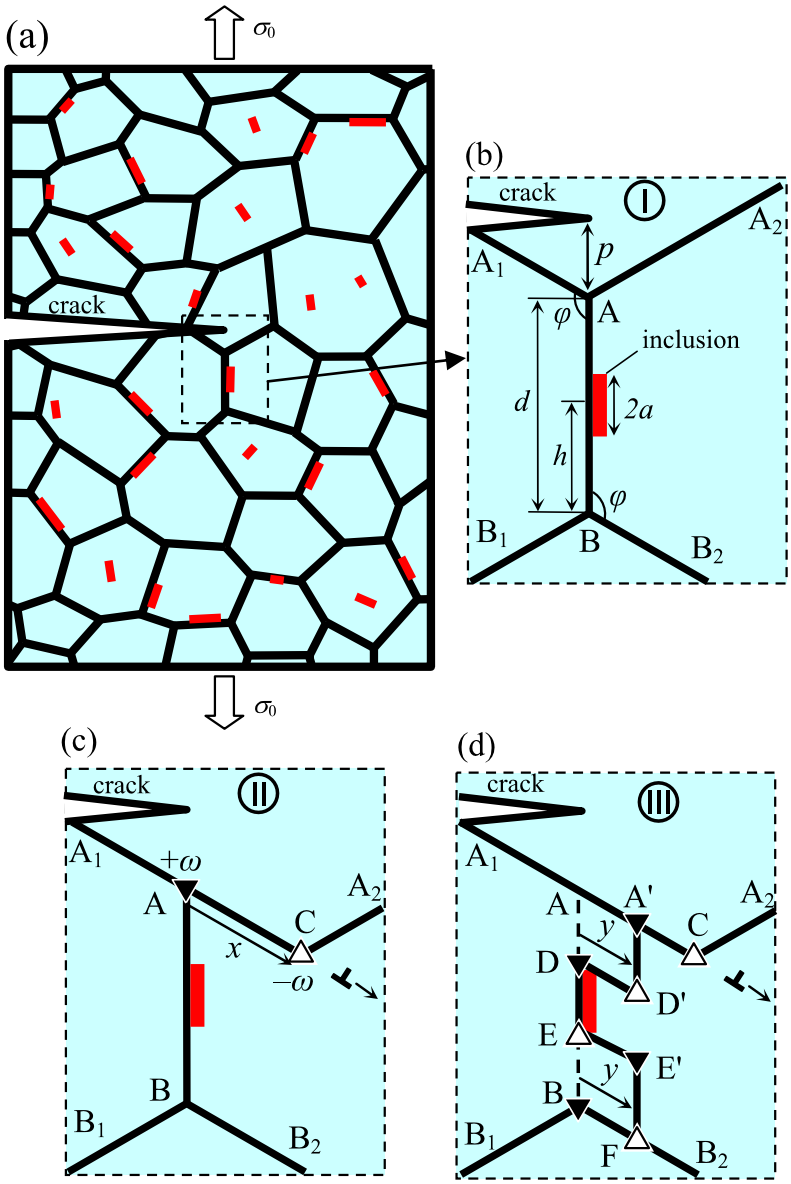

Fig. 1. Grain boundary deformation processes in nanocrystalline specimen with inclusions near a crack tip. (a) General view. (b) Initial configuration I of grain boundaries. (c) Configuration II results from pure grain boundary sliding. Dipole of disclinations AC is generated due to grain boundary sliding. (d) Configuration III results from cooperative grain boundary sliding and migration process. System of 8 disclinations are generated due to this cooperative process.

hancing ductility of material. As was shown in Ref. [30], this cooperative action of GB sliding and migration can effectively increase critical stress intensity factor for crack growth in nanocrystalline metals and ceramics by a factor of 3 or more. The main of this paper is to extend the approach developed in Ref. [30] on the nanostructured materials containing inclusions of second phase to describe operation of the cooperative GB sliding and migration process near crack tips and to theoretically analyze its effect (associated with the local stress relaxation near crack tips) on the fracture toughness.

2. COOPERATIVE GRAIN BOUNDARY SLIDING AND MIGRATION NEAR A CRACK TIP: MODEL

Let us consider the geometric features of cooperative GB sliding and migration in a deformed nanostructured specimen with a crack (Fig. 1). The specimen also contains inclusions dispersed throughout its volume (red rectangles in Fig. 1). For definiteness, we focus our analysis on the situation where the crack is flat, and the specimen is under a tensile load σ_0 normal to the crack plane; that is, a

mode I cracking (Fig. 1a). The applied load and high stress concentration near the crack tip can induce both GB migration and sliding near this tip (Fig. 1). These processes release, in part, the high elastic stresses near the crack tip and thereby can slow down crack growth. Assuming that the intensity of GB migration and sliding and their effect on crack growth strongly increase with a decrease of the distance between the crack tip and GBs involved in these processes, it is reasonable to believe that the dominant effect of GB migration and sliding processes on crack propagation may be determined by these processes near the tip.

The geometry of this deformation mechanism is schematically presented in Fig. 1. Fig. 1a depicts a two-dimensional section of a deformed nanocrystalline specimen. Within the framework of the model [30], GB sliding occurs under the applied shear stress and transforms the initial configuration I of GBs (Fig. 1b) into configuration II (Fig. 1c). GB sliding is assumed to be accommodated, in part, by emission of lattice dislocations from triple junctions (Fig. 1c). Besides, following Refs. [42,43], GB sliding results in the formation of a dipole of wedge disclinations AC in configuration II (Fig. 1c) characterized by strengths $\pm\omega$ with magnitude ω being equal to the tilt misorientation of the GB AB, which is assumed to be a symmetric tilt boundary. The disclination dipole AC has an arm (the distance between the disclinations) equal to the magnitude x of the relative displacement of grains (Fig. 1c).

We further assume [30] that, in parallel with GB sliding, stress-driven GB migration occurs as well, so that the stress fields of defects created by GB sliding are, in part, accommodated by the defects created by GB migration. Unlike the situation in [30], in this case GB migration is partially hindered by the presence of immobile inclusions in the material. For simplicity, we consider here the case where inclusion is located right at the migrating GB. Following the model of GB migration in material with inclusions proposed in Ref. [14], the segment BC of the GB AD stays immobile (due to the presence of the immobile inclusion), whereas the GB segments AD and EB migrate to their new positions A'D' and E'F, respectively. Similar to the model [14] we assume here that both segments migrate simultaneously the same distance y. Stress-driven migration of the GB AB gives rise to the formation of new GB fragments DD' and EE' (Fig. 1d). Besides, for geometric reasons, stress-driven GB migration is accompanied by formation of wedge disclinations at GB junctions [44] (Fig. 1d). Stress-driven migration of the GB AB (Figs. 1d) violates balance of GB misorientation angles at pre-existent and new GB junctions A, B, D, E, A', B', D' and E' so that these junctions contain wedge disclinations (shown as triangles in Fig. 1c) serving as powerful stress sources. All disclinations resulting from both GB sliding and GB migration in Fig. 1 have strengths either $+\omega$ or $-\omega$ (shown as white and black triangles, respectively), where the strength magnitude ω is equal to tilt misorientation of the GB AB. The disclination with the strength $+\omega$ appearing at the point A due to GB sliding and the disclination with the strength $-\omega$ appearing at the same point due to GB migration annihilate, so there is no disclination at point A as shown in Fig. 1d.

As a result, the cooperative GB sliding and migration process transforms the initial configuration I (Fig. 1b) into the final configuration III (Fig. 1d). During this processes, in parallel with GB sliding that causes the relative displacement of grains over the distance x, stress-driven migration of the vertical GB hindered by inclusion occurs (partially) over the distance y (Fig. 1d). The cooperative GB sliding and migration process leads to the formation of 8 wedge disclinations whose positions are specified by parameters x and y.

3. ENERGY CHARACTERISTICS OF COOPERATIVE GRAIN BOUNDARY MIGRATION AND SLIDING PROCESS NEAR CRACK TIP

Let us now consider the effect of the applied tensile load and a long flat mode I crack on the cooperative GB sliding and migration process in a nanocrystalline specimen with inclusions (Fig. 1). The specimen is supposed to be an elastically isotropic solid characterized by the shear modulus G and Poisson's ratio ν. The vertical GB AB is assumed to be normal to the crack growth direction and make an angle φ with the grain boundaries AA1 and BB2 (Fig. 1b). Let the triple junction A lie directly below at a distance p from the crack tip and the length of all GBs in the initial state (Fig. 1b) be denoted as d. Position and size of the inclusion is specified by the following parameters: $2a$ – the length of inclusion (and the GB fragment DE), h – the distance between point B and middle point of the inclusion. Within the framework of proposed model only the length of the inclusion in the direction parallel to the GB plane is important (length in the perpendicular direction is irrelevant). To calculate the parameters of the cooperative GB sliding and migration process, let us first calculate the energy change ΔW associated with the formation of the

disclination configuration shown in Fig. 1d. We use here the results of the work [30], where the scheme for such calculation is developed. The energy change ΔW can be written as:

$$\Delta W = \sum_{j=1}^{8} W^{\Delta}(r_j,\theta_j) + \sum_{j=1}^{7}\sum_{k=j+1}^{8} s_j s_k W_{int}(r_j,r_k,\theta_j,\theta_k) + \sum_{j=1}^{8} s_j W^{\Delta-\sigma}(r_j,\theta_j) + \Delta W_{gb} - A_{sl}, \quad (1)$$

where (r_j,θ_j) are the coordinates of the jth disclination in the polar coordinate system with the origin at the crack tip (j = 1–8; see Fig. 1), and the rest of the symbols are defined as follows: $W^{\Delta}(r_j,\theta_j)$ is the energy of the jth disclination in the solid with a crack, $W_{\text{int}}(r_j, r_k, \theta_j, \theta_k)$ is the energy of the interaction between the jth and kth disclinations assuming that both disclinations have the strength $+\omega$; $W^{\Delta-\sigma}(r_j,\theta_j)$ is the energy of the interaction between the disclination with the strength $+\omega$, lying in the point (r_j,θ_j), and the stress field σ_{il} induced by the applied load near the crack tip; ΔW_{gb} is the change in the GB energy due to the formation of the new GB segments DD' and EE', and A_{sl} is the work of the stress σ_{il} done on GB sliding, which does not account the formation of disclinations. The parameters s_j in Eq. (1) account for the sign of a specified disclination and are defined as $s_1=s_4=s_6=s_8=1$, $s_2=s_3=s_5=s_7=-1$. The coordinates (r_j,θ_j) are calculated as follows:

$$\begin{aligned}
&r_1(y) = (y^2 - 2yp\cos\varphi + p^2)^{1/2},\ \ r_2(x) = (x^2 - 2xp\cos\varphi + p^2)^{1/2},\\
&r_3(y) = (y^2 - 2y(p+d-h-a)\cos\varphi + (p+d-h-a)^2)^{1/2},\ \ r_4 = p+d-h-a,\\
&r_5 = p+d-h+a,\ \ r_6(y) = (y^2 - 2y(p+d-h+a)\cos\varphi + (p+d-h+a)^2)^{1/2},\\
&r_7(y) = (y^2 - 2y(p+d)\cos\varphi + (p+d)^2)^{1/2},\ \ r_8 = p+d,\\
&\theta_j(y) = -\arccos(y\sin\varphi / r_j),\ j = 1,3,6,7,\ \ \theta_2(x) = -\arccos(x\sin\varphi / r_2),\ \ \theta_4 = \theta_5 = \theta_8 = -\pi/2.
\end{aligned} \quad (2)$$

In Eq. (1), we neglected the resistance to GB sliding associated with both the "friction" of the grain boundary AA_1 and the increase of its length in the course of GB sliding. All terms in (1) except ΔW_{gb} are found in Ref. [30]:

$$\begin{aligned}
&W^{\Delta}(r_j,\theta_j) = \frac{G\omega^2 d^2 h(r/d)}{4\pi(1-\nu)},\ \ W_{int}(r_j,r_k,\theta_j,\theta_k) = \frac{G\omega^2 d^2 g(r_j/d, r_k/d, \theta_j,\theta_k)}{4\pi(1-\nu)},\\
&W^{\Delta-\sigma}(r,\theta) = \frac{4\omega K_I^{\sigma}\cos^3(\theta/2)}{3\sqrt{2\pi}},\ \ A_{sl} = -\frac{xK_I^{\sigma}}{2\sqrt{2\pi}}\int_0^d \frac{\sin\theta_2(x')\cos^2(3\theta_2(x')/2 + 2\varphi)}{\sqrt{r_2(x')}}dx',
\end{aligned} \quad (3)$$

where $h(r/d)$ and $g(r_j/d, r_k/d, \theta_j, \theta_k)$ are known functions [45], K_I^{σ} is the stress intensity factor associated with the applied load σ_0. The remaining term ΔW_{gb} is given by:

$$\Delta W_{gb} = 2\gamma_{gb} y, \quad (4)$$

where γ_{gb} is the specific GB energy .

Thus, we have obtained appropriate expressions (2)–(4) for all the energy terms appearing in (1) for the total energy ΔW. The typical dependence $\Delta W(x/d, y/d)$ are shown in Fig. 2, for the exemplary case of Al-based alloy Al-3Mg-0.2Sc, containing Al_3Sc inclusions, and $K_I^{\sigma} = K_{IC}^{br}$, where $K_{IC}^{br} = \sqrt{4G\gamma_e/(1-\nu)}$ is the critical value of the stress intensity factor in the absence of disclinations (that is, in the case of brittle fracture). In general, K_{IC}^{br} depends on γ_e, where $\gamma_e=\gamma$ (with γ being free surface energy) in the case of an intragrain crack, and $\gamma_e = \gamma - \gamma_{gb}/2$ in the case of a intergrain (GB) crack. Fig. 2 presents the plot $\Delta W(x/d, y/d)$ for intergrain crack. In plotting Fig. 2, we used the following values of parameters (for simplicity, we used here values for pure nanocrystalline Al): G = 26.5 GPa, ν = 0.34 [46], γ = 0.54 J/m^2 [47], γ_{gb} = 0.4 J/m^2 [48], $\varphi = 2\pi/3$, d = 50 nm, $p = d$, $\omega = 17°$, $h = 0.5d$, $a = 0.1d$. The curve with arrow in Fig. 2 shows the line of the largest (in magnitude) energy gradient leading to a point M specifying minimum of the energy change ΔW at some equilibrium values $x=x_0$ and $y=y_0$ of the distances of GB sliding and GB migration, respectively. Our analysis shows that general aspects of sliding and migration distances dependences on the various parameters of the system in question is very similar to those discovered in Ref. [30], so we will not discuss

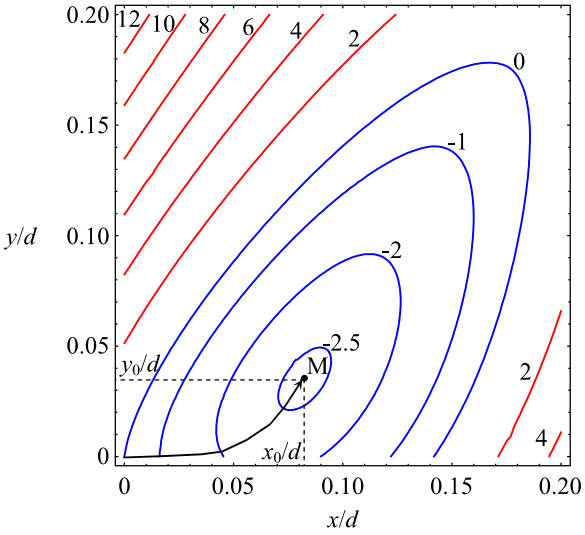

Fig. 2. Contour map of the energy change ΔW associated with the cooperative grain boundary migration and sliding process (near the tip of a large mode I crack in Al-based alloy) in the coordinate space (x/d, y/d), for the case ω=17°, h=0.5, a=0.1d. The energy ΔW is given in units of 10^{-8} J m^{-1}.

them here. In this article we are mainly interested in the aspects of fracture toughness behavior, which are considered in the next section.

4. CRITICAL STRESS INTENSITY FACTOR FOR CRACK GROWTH IN NANOSTRUCTURED SOLID WITH INCLUSIONS

Now let us consider the effect of disclination configuration, resulting from the cooperative GB migration and sliding, on the fracture toughness of a nanocrystalline solid. To do so, we will use the standard crack growth criterion [49] based on the balance between the driving force related to a decrease in the elastic energy and the hampering force related to occurrence of a new free surface during crack growth. In the examined case of the plane strain state, this criterion is given [49] by

$$\frac{1-\nu}{2G}\left(K_I^2 + K_{II}^2\right) = 2\gamma_e, \tag{5}$$

where K_I (mode I) and K_{II} (mode II) are the stress intensity factors for normal (to crack plane) and shear loading, respectively. In the considered situation where the crack growth direction is perpendicular to the direction of the external load, the coefficients K_I and K_{II} are given by the expressions

$$K_I = K_I^\sigma + k_I^q, \quad K_{II} = k_{II}^q, \tag{6}$$

where k_I^σ and k_{II}^σ are the stress intensity factors associated with the internal stresses created by the disclinations located near the crack tip (Fig. 1).

Within the above macroscopic mechanical description, the effect of the local plastic flow – the cooperative GB migration and sliding mechanism resulting in the formation of wedge disclinations – on crack growth can be accounted for through the introduction of the critical stress intensity factor K_{IC}. In this case, the crack is considered as that propagating under the action of the tensile load perpendicular to the crack growth direction, while the presence of the disclinations simply changes the value of K_{IC} corresponding to the case of brittle crack propagation. In these circumstances, the critical condition for the crack growth can be represented as (e.g., Ref. [50]): $K_I^\sigma = K_{IC}$.

Substituting Eq. (6) into Eq. (5) and using the critical condition $K_I^\sigma = K_{IC}$, we find the following expression for K_{IC} [45]:

$$K_{IC} = \sqrt{\left(K_{IC}^{br}\right)^2 - \left(k_{IIC}^q\right)^2} - k_{IC}^q. \tag{7}$$

The quantities in Eq. (7) are defined as follows: $K_{IC}^{br} = \sqrt{4G\gamma_e / (1-\nu)}$, $k_{IIC}^q = k_{II}^q\big|_{K_I^\sigma = K_{IC}}$, and $k_{IC}^q = k_I^q\big|_{K_I^\sigma = K_{IC}}$. It should be noted that the quantities k_{IC}^σ and k_{IIC}^σ depend on K_{IC}, and, thus, Eq. (7) provides the appropriate formula for the determination of K_{IC}.

The quantities k_I^σ and k_{II}^σ appearing in the above expression are given [45] by the following relations:

$$k_I^q = G\omega\sqrt{d} f_1(x,y) / \left[2\sqrt{2\pi}(1-\nu)\right],$$
$$k_{II}^q = G\omega\sqrt{d} f_2(x,y) / \left[2\sqrt{2\pi}(1-\nu)\right],$$

where

$$f_1(x,y) = \sum_{k=1}^{8} s_k \sqrt{r_k / d} \times$$
$$\left[3\cos(\theta_k / 2) + \cos(3\theta_k / 2)\right],$$
$$f_2(x,y) = \sum_{k=1}^{8} s_k \sqrt{r_k / d} \times \tag{8}$$
$$\left[\sin(\theta_k / 2) + \sin(3\theta_k / 2)\right].$$

Using the above expressions, one can numerically solve Eq. (7) for K_{IC} in the following way. For a preset value of K_I^σ, one calculates the energy change ΔW and the equilibrium GB migration distances x_0 and y_0 that correspond to a minimum of ΔW. Substituting the obtained values of x_0 and y_0 into Eq. (8), we deduce the values of k_I^σ and k_{II}^σ. Then we compute the quantities k_{IC}^σ and k_{IIC}^σ with the assumption that $K_I^\sigma = K_{IC}$. On the next step, we calculate

K_{IC} using Eq. (7) and estimate the difference between the so obtained value of K_{IC} and the value of K_I^{σ}. Then we vary the preset value of K_I^{σ} and repeat the above procedure until the value of K_{IC} (given by Eq. (7)) becomes sufficiently close (within specified error margin) to the value of K_I^{σ}.

In order to estimate the effect of the disclinations produced by the cooperative GB migration and sliding process (Fig. 1) on crack growth, one should compare the critical stress intensity factor K_{IC} with the quantity K_{IC}^{br}. To do so, we have calculated the ratio K_{IC}/K_{IC}^{br}. in the cases of nanocrystalline Al-based alloy and nanocomposite Ni-graphene with p=d=50 nm, various values of ω and of the other parameters (for Al-based alloy we used value specific for pure Al; see above); for Ni-graphene composite we used values for pure Ni: G=73 GPa, ν=0.31 [51], γ=1.725 J/m^2, and γ_{gb}=0.69 J/m^2 [46]. In the case of an intragrain crack in Al-based alloy and values of parameters h=0.5d, a=0.1d specifying inclusion size and position, the calculations give the following results. For ω=45°, we obtain $K_{IC}/K_{IC}^{br} \approx 1.31$; for ω=30°, we obtain $K_{IC}/K_{IC}^{br} \approx 1.59$; for ω=15°, we obtain $K_{IC}/K_{IC}^{br} \approx 3.11$. It should be noted that at low enough values of ω (like ω=15°) Eq. (7) cannot be solved with the algorithm described above. It is because at those values of ω the system goes into unstable mode, where both sliding and migration distances grow uncontrollably (as $\Delta W(x,y)$ becomes monotonously decreasing function with no minimum). To obtain ratio K_{IC}/K_{IC}^{br} in those cases we use the same rough estimation as in Ref. [30]: we assume that the length of GB sliding cannot exceed GB length d, manually set equilibrium sliding distance x_0=d and calculate K_{IC}/K^{br}_{IC} using that distance.

In the case of a GB crack in nanocrystalline Al-based alloy, our calculations give the following results. For ω=45°, we obtain $K_{IC}/K_{IC}^{br} \approx 1.29$; for ω=30°, we obtain $K_{IC}/K_{IC}^{br} \approx 1.40$; for ω=15°, we obtain $K_{IC}/K_{IC}^{br} \approx 3.14$. As is seen, for the same values of ω, the values of the ratio K_{IC}/K_{IC}^{br} characterizing a GB crack are very close to those characterizing an intragrain crack.

Similarly, in the case of an intragrain crack in Ni-graphene nanocomposite, one derives the following results. For ω=45°, we obtain $K_{IC}/K_{IC}^{br} \approx 1.36$; for ω=30°, we obtain $K_{IC}/K_{IC}^{br} \approx 1.52$; for ω=15°, we obtain $K_{IC}/K_{IC}^{br} \approx 2.62$. For a GB crack in Ni-graphene nanocomposite, we have $K_{IC}/K_{IC}^{br} \approx 1.34$, 1.48, 2.78, for ω=45°, 30° and 15°, respectively.

Thus, the values of K_{IC}/K_{IC}^{br} in the cases of GB and intragrain cracks are practically the same (at least, for the cases of ω=30° and 45°). With these theoretical estimates, one can conclude that (a) conditions for occurrence of the cooperative GB sliding and migration process near intergrain and intragrain cracks are very similar; (b) the effects of the cooperative GB sliding and migration process on the local stress relaxation near tips of intergrain and intragrain cracks are very similar; and, as a corollary, (c) the effects of the cooperative GB sliding and migration process on crack growth in the cases of intergranular and intragrain fracture processes are very similar.

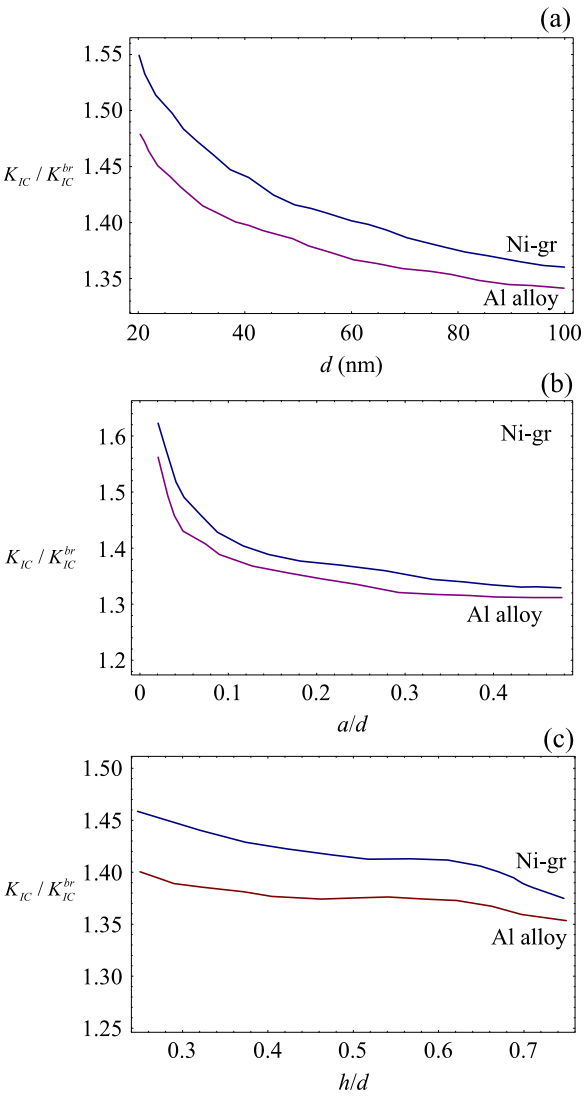

Fig. 3. Dependences of normalized critical stress intensity factor K_{IC}/K_{IC}^{br} in the case of a grain boundary crack in Al-based alloy and Ni-graphene composite on (a) grain size d; (b) inclusion half-length a; (c) parameter h, specifying position of the inclusion relative to grain boundary plane.

Comparison with the results of the earlier model [30] in the case of unhindered by inclusions GB migration shows that presence of inclusions in the materials lowers the value of K_{IC}/K_{IC}^{br} by about 25%,

which is expected as the plasticity associated with GB migration is obviously suppressed by inclusions.

Now let us consider the effect of grain size and parameters characterizing size and positions of inclusions on the critical stress intensity factor K_{IC}. To do so, we calculated the dependence of K_{IC}/K_{IC}^{br} on grain size d in the case of a GB crack in nanocrystalline Al-based alloy and Ni-graphene nanocomposite. The dependences are presented in Fig. 3a, for ω=30°, p=d, h=0.5d, a=0.1d and other parameter values specified above. Fig. 3a demonstrates that, as the grain size increases from 10 to 100 nm, the ratio K_{IC}/K_{IC}^{br} decreases. This tendency allows us to conclude that the suggested cooperative GB sliding and migration mechanism is most effective in fracture toughness enhancement in nanocrystalline materials at finest grain sizes. It is contrasted to the situation with lattice dislocation emission from crack tips – the conventional toughening mechanism in metallic materials [52,53] – whose enhancing effect on the fracture toughness of nanocrystalline metals rapidly decreases with a decrease in grain size [54].

Fig. 3b presents dependences of K_{IC}/K_{IC}^{br} on the inclusion half-length a calculated for ω=30°, d=50 nm, p=d, h=0.5d. Fig. 3b demonstrates that ratio K_{IC}/K_{IC}^{br} monotonously decreases with increasing length of the inclusion, which is consistent with the results obtained in Ref. [14] showing that GB migration (expressed in the form of equilibrium migration distance) is suppressed for longer inclusion. Fig. 3c shows dependences of K_{IC}/K_{IC}^{br} on the parameter h specifying position of the inclusion relative to GB plane (see Fig. 1). This figure demonstrates that critical stress intensity factor weakly depends on the inclusion position relative to GB plane with slight tendency to decreasing with increasing parameter h. So main conclusion we can make here is that the primary factor affecting fracture toughness is the inclusion size: the smaller the inclusion size the bigger is the ratio K_{IC}/K_{IC}^{br}. Comparison with the results of work [30] shows that the presence of inclusions lowers the ratio K_{IC}/K_{IC}^{br} by a factor of about 25% compared to a materials without inclusions.

Thus, the results of our calculations show that cooperative GB migration and sliding along a single GB can make the critical stress intensity factor K_{IC} several times larger. Apparently, cooperative GB migration and sliding along various GBs can increase the value of K_{IC} much further and, as a result, may lead to a significant increase of fracture toughness, as compared to the case of pure brittle fracture.

5. CONCLUDING REMARKS

We have theoretically described the cooperative GB sliding and migration process near crack tips and its effect on the growth of sufficiently large cracks in deformed nanostructured metals with inclusions of the second phase. The cooperative GB sliding and migration deformation mechanism is shown to increase the critical stress intensity factors by several times and, as a result, it may lead to a significant enhancement of fracture toughness of these materials. This mechanism is equally effective for growth suppression of both intra- and intergranular cracks.

The presence of inclusions lowers the ratio K_{IC} by a factor of about 25% compared to a materials without inclusions due to obvious suppression of plasticity by inclusions serving as obstacles to GB migration. Most important parameter affecting fracture toughness is the inclusion size, while position of the inclusion relative to GB plane is not very important.

In general, several deformation mechanisms – lattice dislocation slip, GB sliding, stress-driven GB migration as well as rotational deformation modes and other – can contribute to plastic deformation in nanocrystalline materials and may thus result in fracture toughness enhancement of such materials. The effect of each mechanism on the fracture toughness of a nanocrystalline specimen depends on the structure of the specimen and its loading conditions. It is the effective combined action of various deformation mechanisms at certain conditions that can provide the experimentally observed high fracture toughness of nanocrystalline metals and ceramics.

ACKNOWLEDGEMENTS

This work was supported, in part (for SVB), by the Russian Ministry of Education and Science (grant 14.B25.31.0017 and Zadanie 16.3483.2017/PCh), in part (for ASK), by the Council for grants of the President of Russian Federation (grant MD-3154.2017.1), and, in part (for NVS), by the Ministry of Education and Science of Russian Federation (grant MD-9152.2016.1) and the Russian Fund of Basic Research (grant 16-32-60110).

REFERENCES

[1] E.C. Aifantis // *Mater. Sci. Eng. A* **503** (2009) 190.

[2] M. Dao, L. Lu, R.J. Asaro, J.T.M. De Hosson and E. Ma // *Acta Mater.* **55** (2007) 4041.

[3] J.R. Greer and J.T.M. De Hosson // *Prog. Mater. Sci.* **56** (2011) 654.
[4] M. Kawasaki and T.G. Langdon // *J. Mater. Sci.* **51** (2016) 19.
[5] C.C. Koch, I.A. Ovid'ko, S. Seal and S. Veprek, *Structural Nanocrystalline Materials: Fundamentals and Applications* (Cambridge University Press, Cambridge, 2007).
[6] P. Kumar, M. Kawasaki and T.G. Langdon // *J. Mater. Sci.* **51** (2016) 7.
[7] I.A. Ovid'ko and T.G. Langdon // *Rev. Adv. Mater. Sci.* **30** (2012) 103.
[8] R.Z. Valiev, A.P. Zhilyaev and T.G. Langdon, *Bulk Nanostructured Materials: Fundamentals and Applications* (Wiley, Hoboken, New Jersey, USA, 2014).
[9] R.Z. Valiev and Y.T. Zhu // *Trans. MRS Japan* **40** (2015) 309.
[10] Y.T. Zhu, X.Z. Liao and X.L. Wu // *Prog. Mater. Sci.* **57** (2012) 1.
[11] S.V. Bobylev, N.F. Morozov and I.A. Ovid'ko // *Phys. Rev. Lett.* **105** (2010) 055504.
[12] S.V. Bobylev, N.F. Morozov and I.A. Ovid'ko // *Phys. Rev. B* **84** (2011) 094103.
[13] S.V. Bobylev, N.F. Morozov and I.A. Ovid'ko // *Rev. Adv. Mater. Sci.* **48** (2017) 131.
[14] S.V. Bobylev, N.F. Morozov and I.A. Ovid'ko // *Dokl. Phys.* **62** (2017) 124.
[15] S.V. Bobylev and I.A. Ovid'ko // *Phys. Rev. Lett.* **109** (2012) 175501.
[16] S.V. Bobylev and I.A. Ovid'ko // *Acta Mater.* **88** (2015) 260.
[17] S.V. Bobylev and I.A. Ovid'ko // *Acta Mater.* **124** (2017) 333.
[18] S.V. Bobylev and I.A. Ovid'ko // *Rev. Adv. Mater. Sci.* **50** (2017) 104.
[19] J.T.M. De Hosson, W.A. Soer, A.M. Minor, Z.W. Shan, E.A. Stach, S.A. Syed Asif and O.L. Warren // *J. Mater. Sci.* **41** (2006) 7704.
[20] V. Dupont and F. Sansoz // *Acta Mater.* **56** (2008) 6013.
[21] D. Farkas, A. Frøseth and H. Van Swygenhoven // *Scr. Mater.* **55** (2006) 695.
[22] D.S. Gianola, S. Van Petegem, M. Legros, S. Brandstetter, H. Van Swygenhoven and K.J. Hemker // *Acta Mater.* **54** (2006) 2253.
[23] D.S. Gianola, D.H. Warner, J.F. Molinari and K.J. Hemker // *Scr. Mater.* **55** (2006) 649.
[24] M.Y. Gutkin and I.A. Ovid'ko // *Appl. Phys. Lett.* **87** (2005) 251916.
[25] M. Jin, A.M. Minor, E.A. Stach and J.W. Morris // *Acta Mater.* **52** (2004) 5381.
[26] X.Z. Liao, A.R. Kilmametov, R.Z. Valiev, H.S. Gao, X.D. Li, A.K. Mukherjee, J.F. Bingert and Y.T. Zhu // *Appl. Phys. Lett.* **88** (2006) 021909.
[27] Y.J. Lin, H.M. Wen, Y. Li, B. Wen, W. Liu and E.J. Lavernia // *Acta Mater.* **82** (2015) 304.
[28] I.A. Ovid'ko and A.G. Sheinerman // *Rev. Adv. Mater. Sci.* **39** (2014) 99.
[29] I.A. Ovid'ko and A.G. Sheinerman // *J. Mater. Sci.* **50** (2015) 4430.
[30] I.A. Ovid'ko, A.G. Sheinerman and E.C. Aifantis // *Acta Mater.* **59** (2011) 5023.
[31] I.A. Ovid'ko and A.G. Sheinerman // *Acta Mater.* **121** (2016) 117.
[32] I.A. Ovid'ko, A.G. Sheinerman and E.C. Aifantis // *Acta Mater.* **56** (2008) 2718.
[33] F. Sansoz and V. Dupont // *Appl. Phys. Lett.* **89** (2006) 111901.
[34] J.A. Sharon, P.-C. Su, F.B. Prinz and K.J. Hemker // *Scr. Mater.* **64** (2011) 25.
[35] W.A. Soer, J.T.M. De Hosson, A.M. Minor, J.W. Morris and E.A. Stach // *Acta Mater.* **52** (2004) 5783.
[36] Y.J. Lin, H.M. Wen, Y. Li, B. Wen, W. Liu and E.J. Lavernia // *Metall. Mater. Trans. B* **45** (2014) 795.
[37] Y.J. Lin, B.C. Xu, Y.Z. Feng and E.J. Lavernia // *J. Alloy Compd.* **596** (2014) 79.
[38] J. Cizek, I. Prochazka, B. Smola, I. Stulikova, M. Vlach, V. Ocenasek, O.B. Kulyasova and R.K. Islamgaliev // *Int. J. Mater. Res.* **100** (2009) 780.
[39] K. Dám, P. Lejček and A. Michalcová // *Mater. Charact.* **76** (2013) 69.
[40] Z. Horita, M. Furukawa, M. Nemoto, A.J. Barnes and T.G. Langdon // *Acta Mater.* **48** (2000) 3633.
[41] D. Nagahama, D.H. Ping, M. Ohnuma, H. Sasaki, K. Kita and K. Hono // *Mater. Trans.* **44** (2003) 1955.
[42] I.A. Ovid'ko and A.G. Sheinerman // *Appl. Phys. Lett.* **90** (2007) 171927.
[43] I.A. Ovid'ko and A.G. Sheinerman // *Acta Mater.* **57** (2009) 2217.
[44] A.E. Romanov and V.I. Vladimirov, In: *Dislocations in solids*, vol. 9, ed. by F.R.N. Nabarro (North Holland, Amsterdam, 1992), p. 191.
[45] N.F. Morozov, I.A. Ovid'ko, A.G. Sheinerman and E.C. Aifantis // *J. Mech. Phys. Solids* **58** (2010) 1088.

[46] J.P. Hirth and J. Lothe, *Theory of dislocations* (Wiley, New York, 1982).
[47] G.E. Beltz, D.M. Lipkin and L.L. Fischer // *Phys. Rev. Lett.* **82** (1999) 4468.
[48] A.P. Sutton and R.W. Balluffi // *Acta Metall.* **35** (1987) 2177.
[49] G.R. Irwin // *J. Appl. Mech.* **24** (1957) 361.
[50] *Mechanics of Fracture and Strength of Materials*, vol. 2, ed. by V.V. Panasyuk (Naukova Dumka, Kiev, 1988).
[51] C.J. Smithells and E.A. Brands, *Metals reference book* (Butterworth, London, 1976).
[52] J.R. Rice // *J. Mech. Phys. Solids* **40** (1992) 239.
[53] J.R. Rice and R. Thomson // *Philos. Mag.* **29** (1974) 73.
[54] I.A. Ovid'ko and A.G. Sheinerman // *Acta Mater.* **58** (2010) 5286.